UNIVERSITY OF WEST BOHEMIA

Applied and Computational Mechanics 1 (2007) 693 - 702

Applied and Computational Mechanics

Analysis of blood flow through a three-dimensional bypass model

J. Vimmr[a,*], A. Jonášová[a]

[a] *Department of Mechanics, Faculty of Applied Sciences, UWB in Pilsen, Univerzitní 22, 306 14 Plzeň, Czech Republic*

Received 7 September2007; received in revised form 10 October 2007

Abstract

The purpose of this study is to analyze the steady laminar blood flow through a complete idealized three-dimensional bypass model with regard to the bypass hemodynamics and to compare the obtained results with the ones from the two-dimensional model. The type of flow restriction in the native artery is represented by either an occlusion or a 75% symmetric stenosis. In both cases, the blood is considered to be an incompressible Newtonian fluid. The walls are assumed to be impermeable and rigid. In order to solve the non-linear system of incompressible Navier-Stokes equations, the pseudo-compressibility method and the finite volume formulation of the central explicit fourth order Runge-Kutta scheme are applied using own computational software developed for unstructured hexahedral grids.

Keywords: 3D bypass model, hemodynamics, unstructured hexahedral grid, pseudo-compressibility method, FVM

1. Introduction

The application of bypass grafts in medicine is connected with the atherosclerosis of the cardiovascular system. Although the creation of a detour around the damaged artery segment can ensure the needed blood flow, the further bypass patency is strongly dependent on the graft material and the used surgery technique. The failure rates of venous and synthetic bypass grafts are mentioned between 40 to 50% ten years after the implantation.

One of the most common reasons for the late bypass failure is the reduction of inner diameter at the distal anastomosis between the native artery and the bypass graft. The thickening of tunica intima is caused by the development of intimal hyperplasia (IH), a response of the vessel to wall injury. Several studies have proven that the development of IH in bypasses is a consequence of physiological response to abnormal conditions of local hemodynamics. In order to determine the effect of non-uniform flow on the blood cells and the vessel wall, numerous studies were devoted to numerical simulations of the steady and unsteady blood flow in idealized and realistic models with end-to-side bypass graft. For example, [8] investigated the steady blood flow through an occluded bypass model in dependance on various inlet Reynolds numbers and junction angles. Similar problem with the exception of unsteady blood flow in a distal anastomosis was introduced in [5], whereas some of the results were compared with experimental data. In [2], the importance of so-called distance of grafting is illustrated on a distal bypass section with stenosed native artery. Some studies even dealt with the less common grafting techniques such as the side-to-side connection in [3], which is usually used by sequential bypasses. Although numerical simulations may predict changes in flow distributions and patterns

*Corresponding author. Tel.: +420 377 632 314, e-mail: jvimmr@kme.zcu.cz.

and enable the surgeons an insight into the bypass hemodynamics, comparisons against experiments are still needed as it is shown in [1] and [7]. Both studies present the in-vitro results obtained from configurations, which either represent the distal anastomosis or even a complete bypass including the proximal part of the native artery.

The aim of this study is to model a steady laminar blood flow through an idealized three-dimensional bypass model, whose native artery is either occluded or stenosed. Next, the results obtained from the 3D numerical simulations are compared with the already published results of blood flow in 2D bypass models of similar geometry, [10]. Compared to the above mentioned studies, [2] and [5], the model included both the proximal and distal bypass sections in order to analyze the flow development in the entire bypass. The basic geometry of an occluded bypass was taken from [8] with the exception that we extended our computation with the case, when the native artery is still narrowed and a residual flow through the stenosis may influence the flow field in the distal anastomosis. Even though vessel narrowings do not have an unique shape, it is a common practice to describe the stenosis by a cosine function. In our case, we have chosen the Gaussian function, which enabled us to model a more natural reduction of the artery diameter. Another improvement, compared to [8], is the use of more realistic computational parameters, which correspond to a real coronary artery, i.e. $D_{artery} = 3.3\,\mathrm{mm}$ and $Re_{inlet} = 230$. All numerical simulations were implemented by the application of own computational algorithm, which was developed for unstructured hexahedral grids using the finite volume method (FVM).

2. Problem formulation

In this study, an idealized three-dimensional bypass model was considered. The shape of the model corresponds to the in medicine applied coronaro-coronary bypass with the junction angle $45°$. The diameter of the connected end-to-side bypass graft was set equal to the coronary artery ($D = 3.3\,\mathrm{mm}$), whose length was $L = 50\,\mathrm{mm}$. The flow restriction in the middle of the native artery had either the form of a symmetric 75% stenosis or of an occlusion, see fig. 1. The shape of the artery narrowing was described by the Gaussian function. Compared to this, the vessel occlusion did not require a special shape, and therefore, it was modelled as a wall,

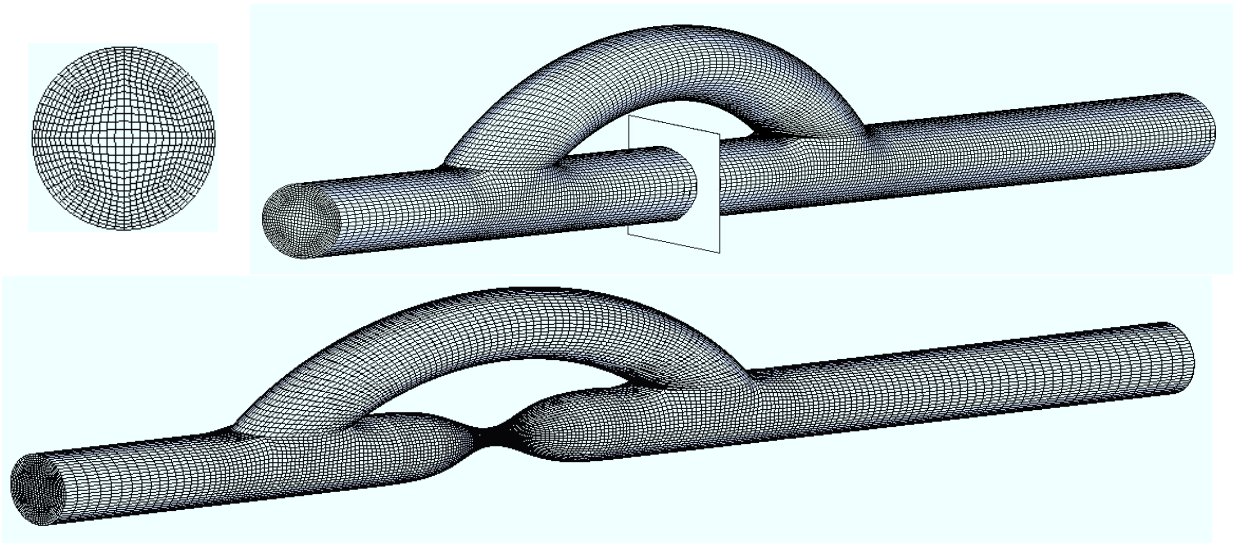

Fig. 1. Computational grids - occluded bypass with the marked artery obstruction (above) and stenosed bypass (bellow); computational grid in the native artery cross-section (left).

which divided the straight tube into the proximal and distal artery segments. Since the most common used grafts are veins and synthetic protheses, both with negligible elastic properties, we assumed the walls to be impermeable and rigid. The blood flow was supposed to be an isothermal laminar flow of incompressible Newtonian fluid with the density $\rho = 1050\,\mathrm{kg\,m^{-3}}$ and the molecular viscosity $\eta = 0.0042\,\mathrm{Pa\,s}$. We considered the flow to be steady, since the purpose of this study was only to analyze the geometry influence on the flow uniformity inside the bypass model.

Compared to the two-dimensional case, whose grid generation is relatively simple, both three-dimensional bypass models required more detailed grid preparation with regards to the needed refinement in the wall vicinity and the problematic connection of both tubes. One of possible solutions is the generation of an unstructured hexahedral grid, which in our case could be achieved using the software package Altair Hypermesh. The computational grid in the native artery cross-section is visible in fig. 1. Although the use of unstructured hexahedral grid partly facilitated the meshing process, the development of own computational software based on the cell-centred FVM had to be adapted not only to the unstructured grid, but also to the data output from the commercial software package Altair Hypermesh. The node coordinates and the elements with corresponding node numbers served as the source data for further processing. The principle of this process consisted in the organization of the computational grid, i.e. it was necessary to determine the neighbouring finite volumes and to prescribe boundary conditions at corresponding faces. In this sense, a relatively universal computational software could be achieved, whose algorithm may be easily modified in the future in order to perform numerical simulations in more complex geometries using tetrahedral cells.

3. Mathematical model and numerical method

Let us consider a computational domain $\Omega \subset \mathbb{R}^3$ with the boundary $\partial\Omega$ and a time interval $(0, \mathcal{T})$ with $\mathcal{T} > 0$. The non-linear conservative system of the incompressible Navier-Stokes (NS) equations for a three-dimensional steady laminar flow after the application of the pseudo-compressibility method, proposed by Chorin [4], is expressed in the compact flux vector form as

$$\frac{\partial \boldsymbol{w}}{\partial t} + \frac{\partial}{\partial y^j}\boldsymbol{\mathcal{H}}^j(\boldsymbol{w}) - \frac{\partial}{\partial y^j}\boldsymbol{\mathcal{H}}_V^j(\boldsymbol{w}) = \boldsymbol{0} \tag{1}$$

for $j = 1, 2, 3$ in the space-time cylinder $\Omega_T = \Omega \times (0, \mathcal{T})$. The vector $\boldsymbol{w}$ of conservative variables and the tensors of inviscid and viscous fluxes $\boldsymbol{\mathcal{H}}(\boldsymbol{w}) = (\boldsymbol{\mathcal{H}}^1(\boldsymbol{w}), \boldsymbol{\mathcal{H}}^2(\boldsymbol{w}), \boldsymbol{\mathcal{H}}^3(\boldsymbol{w}))$ and $\boldsymbol{\mathcal{H}}_V(\boldsymbol{w}) = (\boldsymbol{\mathcal{H}}_V^1(\boldsymbol{w}), \boldsymbol{\mathcal{H}}_V^2(\boldsymbol{w}), \boldsymbol{\mathcal{H}}_V^3(\boldsymbol{w}))$, respectively, are defined as

$$\begin{aligned}
\boldsymbol{w} &= \left[P,\, v^1,\, v^2,\, v^3\right]^T, \\
\boldsymbol{\mathcal{H}}^j(\boldsymbol{w}) &= \left[\beta^2\, v^j,\, v^j v^1 + P\delta^{1j},\, v^j v^2 + P\delta^{2j},\, v^j v^3 + P\delta^{3j}\right]^T, \\
\boldsymbol{\mathcal{H}}_V^j(\boldsymbol{w}) &= \nu \left[0,\, \frac{\partial v^1}{\partial y^j},\, \frac{\partial v^2}{\partial y^j},\, \frac{\partial v^3}{\partial y^j}\right]^T,
\end{aligned}$$

where $\boldsymbol{y} = [y^1, y^2, y^3]^T$ is the vector of space coordinates, $\boldsymbol{v} = [v^1, v^2, v^3]^T$ is the velocity vector, δ^{ij} is the Kronecker delta, $P = p/\rho$, p is the static pressure and $\nu = \eta/\rho$ is the kinematic viscosity.

To solve the system of the incompressible NS equations in pseudo-transient form (1), the cell-centred finite volume formulation of the central explicit fourth order Runge-Kutta (RK)

scheme was used on an unstructured grid. The applied grid consisted of non-overlapping hexahedral finite volumes Ω_j, $j \in J$, where $J = \{1, 2, \ldots, N\}$ was the index set. Two finite volumes Ω_i, Ω_j, $i, j \in J$ were called neighbours, if $\Gamma_{ij} = \partial\Omega_i \cap \partial\Omega_j = \Gamma_{ji}$, where Γ_{ij} was the quadrilateral face of Ω_i. According to this notation, the algorithm of the RK scheme may be written as

$$\boldsymbol{w}_j^{(1)} = \boldsymbol{w}_j^n \,, \tag{2}$$

$$\boldsymbol{w}_j^{(r+1)} = \boldsymbol{w}_j^n - \alpha_r \,\Delta t\, \mathcal{R}\boldsymbol{w}_j^{(r)} + \mathcal{D}\boldsymbol{w}_j^n \qquad \text{for} \quad r = 1, 2, 3 \,, \tag{3}$$

$$\boldsymbol{w}_j^{n+1} = \boldsymbol{w}_j^n - \frac{\Delta t}{6}\left(\mathcal{R}\boldsymbol{w}_j^{(1)} + 2\mathcal{R}\boldsymbol{w}_j^{(2)} + 2\mathcal{R}\boldsymbol{w}_j^{(3)} + \mathcal{R}\boldsymbol{w}_j^{(4)}\right) + \mathcal{D}\boldsymbol{w}_j^n \,, \tag{4}$$

where $\alpha_1 = 0.5$, $\alpha_2 = 0.5$, $\alpha_3 = 1$ and $\boldsymbol{w}_j^n$ is the approximation of the vector $\boldsymbol{w}$ over the finite volume Ω_j, $j \in J$ at the time level n. The stationary residuum is defined as

$$\mathcal{R}\boldsymbol{w}_j^{(r)} = \frac{1}{|\Omega_j|}\sum_{m=1}^{6}\boldsymbol{\mathcal{H}}_m(\boldsymbol{w}^{(r)})\,\boldsymbol{S}_j^m - \frac{1}{|\Omega_j|}\sum_{m=1}^{6}\boldsymbol{\mathcal{H}}_{Vm}(\boldsymbol{w}^{(r)})\,\boldsymbol{S}_j^m \,,$$

where $|\Omega_j|$ denotes the volume of the hexahedral cell Ω_j and $\boldsymbol{S}_j^m$ is one of the six outer vectors normal to $\partial\Omega_j$, e.g. $\boldsymbol{S}_j^1 = \boldsymbol{S}_{jk} = (S_{jk}^x, S_{jk}^y, S_{jk}^z)^T$ is normal to $\partial\Omega_j$ on the face Γ_{jk}. Consequently, the inviscid numerical flux $\boldsymbol{\mathcal{H}}_1^s(\boldsymbol{w}^{(r)})$, $s = 1, 2, 3$ through the face Γ_{jk} is evaluated as

$$\boldsymbol{\mathcal{H}}_1^s(\boldsymbol{w}^{(r)}) = \frac{1}{2}\left(\boldsymbol{\mathcal{H}}^s(\boldsymbol{w}_j^{(r)}) + \boldsymbol{\mathcal{H}}^s(\boldsymbol{w}_k^{(r)})\right) \,,$$

where $\boldsymbol{w}_j^{(r)}$ and $\boldsymbol{w}_k^{(r)}$ are the approximate solutions on the finite volumes Ω_j and Ω_k, respectively. The remaining inviscid numerical fluxes are computed similarly using the indices of neighbouring finite volumes at corresponding faces. Analogous to the two-dimensional case, the determination of viscous numerical fluxes $\boldsymbol{\mathcal{H}}_m^s(\boldsymbol{w}^{(r)})$, $s = 1, 2, 3$ is based on the application of dual cells, which in the space have the form of octahedrons, fig. 2. For more details see [9].

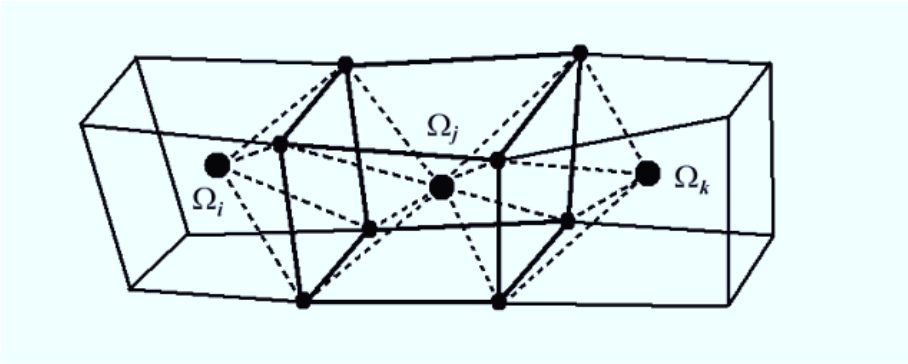

Fig. 2. Finite volume Ω_j with its neighbours Ω_i and Ω_k and corresponding dual cells.

In order to stabilize the numerical solution, an artificial viscosity was added to the computation at each stage of the RK scheme, whereas the dissipative term was calculated only once at the time level n, for details see [6]. For our numerical simulations, we have chosen the Jameson's artificial dissipation, which written in the sense of the finite difference method for the one-dimensional case takes the following form

$$D\boldsymbol{w}_i = \varepsilon_2(\boldsymbol{w}_{i-1}^n - 2\boldsymbol{w}_i^n + \boldsymbol{w}_{i+1}^n) + \varepsilon_4(\boldsymbol{w}_{i-2}^n - 4\boldsymbol{w}_{i-1}^n + 6\boldsymbol{w}_i^n - 4\boldsymbol{w}_{i+1}^n + \boldsymbol{w}_{i+2}^n) \,, \tag{5}$$

where ε_2, $\varepsilon_4 \in \mathbb{R}$ are small constants. A corresponding adaptation of this higher-order artificial viscosity was implemented for the applied unstructured three-dimensional grids.

4. Numerical results

The blood flow through an idealized three-dimensional bypass model was numerically simulated for both considered artery restrictions (occlusion and stenosis). The number of hexahedral cells was equal for the two bypass types ($N_{3D} = 195840$). In all computations presented here, the inlet Reynolds number was set $Re = \bar{U} D \rho / \eta = 230$, which corresponds to the mean Reynolds number in a coronary artery ($\bar{U} \simeq 0.279\,\mathrm{m\,s^{-1}}$). The boundary conditions were identical for both considered three-dimensional models. Inlet: $u = 0\,\mathrm{m\,s^{-1}}$, $v = 0\,\mathrm{m\,s^{-1}}$ and $w(r) = 2\,\bar{U}\left[1 - (2\,r/D)^2\right]$, where $r = \sqrt{x^2 + y^2}$; outlet: a constant pressure $p_2 = 11550\,\mathrm{Pa}$; rigid walls: the non-slip boundary conditions.

The resulting velocity profiles in the longitudinal section together with the iso-velocity contours at selected cross-sections of the occluded 3D bypass are shown in fig. 3. For comparison, similar velocity profiles in the two-dimensional model are enclosed, fig. 4. The blood flow through the idealized bypass model has a particular pattern, which is characterized by the presence of recirculation zones and secondary flows in certain regions. Looking at the iso-velocity contours, it is possible to describe the flow development corresponding to the bypass geometry. At the inlet (A1), the fully developed velocity profile is gradually redirected from the native artery into the graft inlet (A2), whereas a part of the fluid splits and continues towards the occlusion (A3) forming a well-developed recirculation zone. Inside the bypass graft at the beginning, the velocity profile becomes strongly skewed to the lower wall and the contours take a typical 'M' shape (B1), which was also observed in [8]. As the fluid progresses through the bypass graft, the velocity peak shifts towards the tube center (B2) and later on towards the upper wall (B3). Finally, the maximal velocity magnitude is reached at the anastomosis (C1) between the bypass graft and the native artery. Downstream from this region, the flow demonstrates a strong downwash towards the bed of the native artery, which results in a small recirculation zone at the upper wall (C2). Along the distal artery, the flow is gradually stabilized, which is evident from the developing velocity profile at the outlet.

The distribution of recirculation and low-velocity zones along the 3D bypass model are shown in fig. 5. The dark grey color represents the areas, where the flow is either stagnant or the values of velocity magnitude are very low ($|\boldsymbol{v}| < 0.01\,\bar{U}$). The overall flow field in both 2D and 3D models contains four regions, where the fluid recirculates or is almost motionless. Two of the recirculation zones are located in the native artery up- and downstream from the occlusion, whereas their size and velocity depends on the occlusion position between the proximal and distal anastomoses (distance of grafting). The third one can be found not so far from the graft inlet at the upper wall, where it partly extends into the tube along the main stream. The last recirculation zone is situated in the distal artery next to the so called toe (see C2), a part of the anastomosis, where the main stream is accelerated when leaving the bypass graft.

So far the results between the two- and three-dimensional cases are relatively similar. However, taking the effect of the spatial flow into account, the size and the average velocity of this zones differ considerably between both models. For example, the large recirculation region before the occlusion, which is in the three-dimensional model represented by the cross-section marked as A3 or is evident in fig. 5, could not be entirely registered in the two-dimensional case. The average velocity of this structure varies from $0.16\,\bar{U}$ to $0.20\,\bar{U}$, which compared to the remaining recirculation zones ($|\boldsymbol{v}| < 0.10\,\bar{U}$) is quite high. This effect is partly caused by the situation at the upper wall, where the main stream enters the bypass graft and a portion of the fluid is split and flows toward the occlusion with relatively high velocity magnitude around $0.45\,\bar{U}$. On the contrary, the region downstream from the occlusion consists mostly of motion-

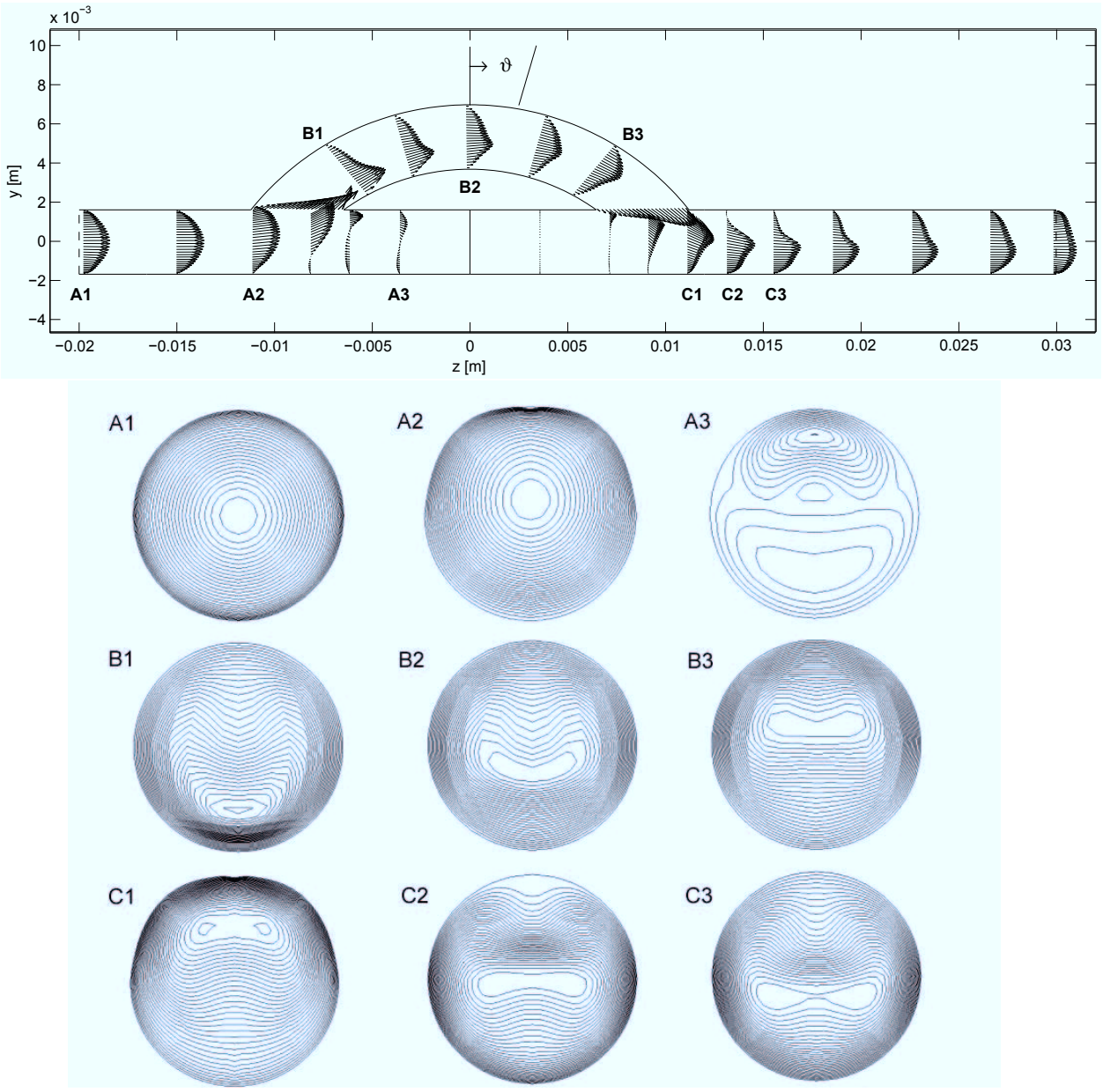

Fig. 3. Velocity profiles in the longitudinal section and iso-velocity contours at selected cross-sections in the occluded 3D bypass.

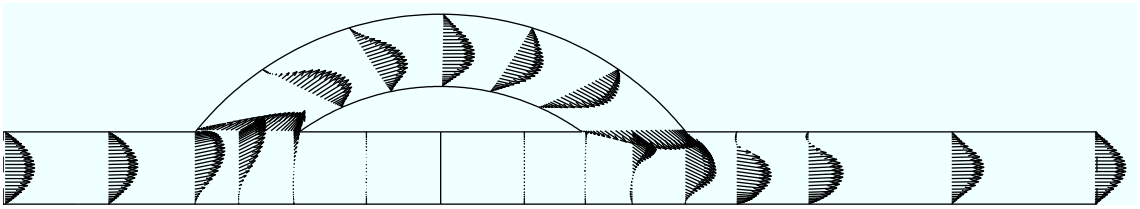

Fig. 4. Velocity profiles at selected cross-sections in the occluded 2D bypass.

less fluid, which near the main stream is disturbed by small recirculation zones near the lower and upper wall of the distal artery.

When investigating the influence of local hemodynamics on the occurrence of intimal hyperplasia at the distal anastomosis, it is important to consider several factors that are associ-

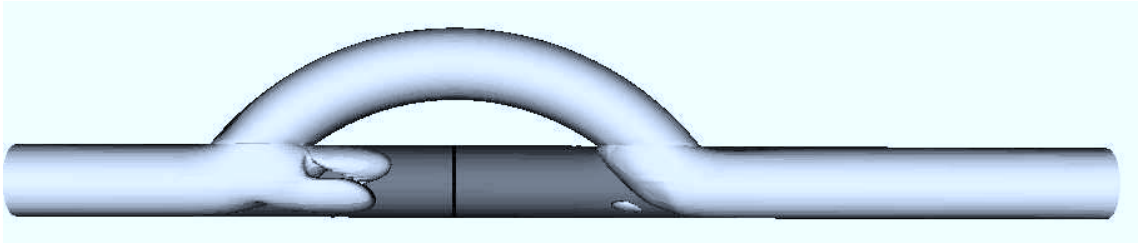

Fig. 5. Distribution of recirculation and low-velocity zones in the occluded 3D bypass.

ated with the non-uniform blood flow. Beside the occurrence of recirculation and low-velocity zones, it is usually necessary to include the distribution of wall shear stress (WSS) into the result analysis. In this study, the graphs of WSS for the occluded artery and the bypass graft in the three-dimensional model are shown in fig. 6. The angle ϑ in the second graph denotes the position along the bypass graft. It is measured form the center of the tube curvature as is shown in fig. 3, whereas in the first half of the bypass graft, the angle values are negative.

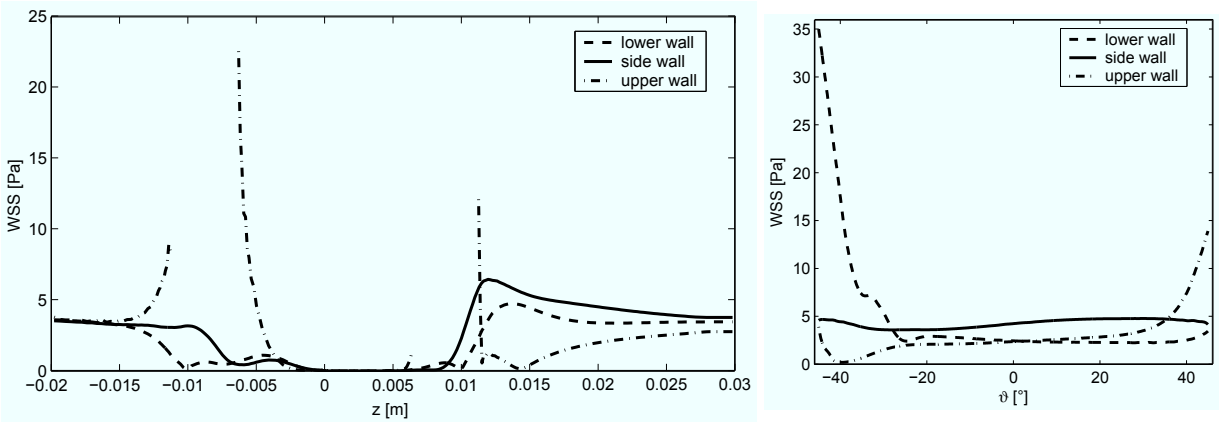

Fig. 6. Graphs of WSS in the occluded 3D bypass - native artery (left), bypass graft (right).

Considering the graphs for the native artery and the bypass graft, the shear stress distribution at selected walls demonstrates the flow development in response to the bypass geometry. In the vicinity of the inlet, when the flow is still a fully developed velocity profile, the WSS distribution is relatively uniform. The changes at all walls begin before the bifurcation, when the main stream is gradually redirected into the bypass graft. The upper artery wall experiences elevated shear stress and reaches a peak value at the corner of the branch. At the opposite corner of the proximal anastomosis, the WSS decreases from a maximum to almost non-existent values. At the lower wall, the shear stress decreases relatively fast to a zero value indicating the position of a stagnation point (around $z = -0.01$ m). Right from this point, the presence of a recirculation zone near the lower wall causes a mild value increase. Compared to the changes at the lower wall, the shear stress at the side wall in the branching region has a similar development. In the distal artery, the presence of a stagnant fluid next to the occlusion is the cause of extremely low WSS values on all three considered bypass walls. Similar to the situation in the proximal artery, a stagnation point at the lower wall divides the tube into two regions. The first one is occupied by a low-velocity recirculation zone and the second is represented by the strong flow impact on the artery bed, which is firstly visible on the side wall. The WSS distribution around the toe at the upper wall, which is characterized by the proximity of high- and low-WSS regions, indicates the presence of a small recirculation zone.

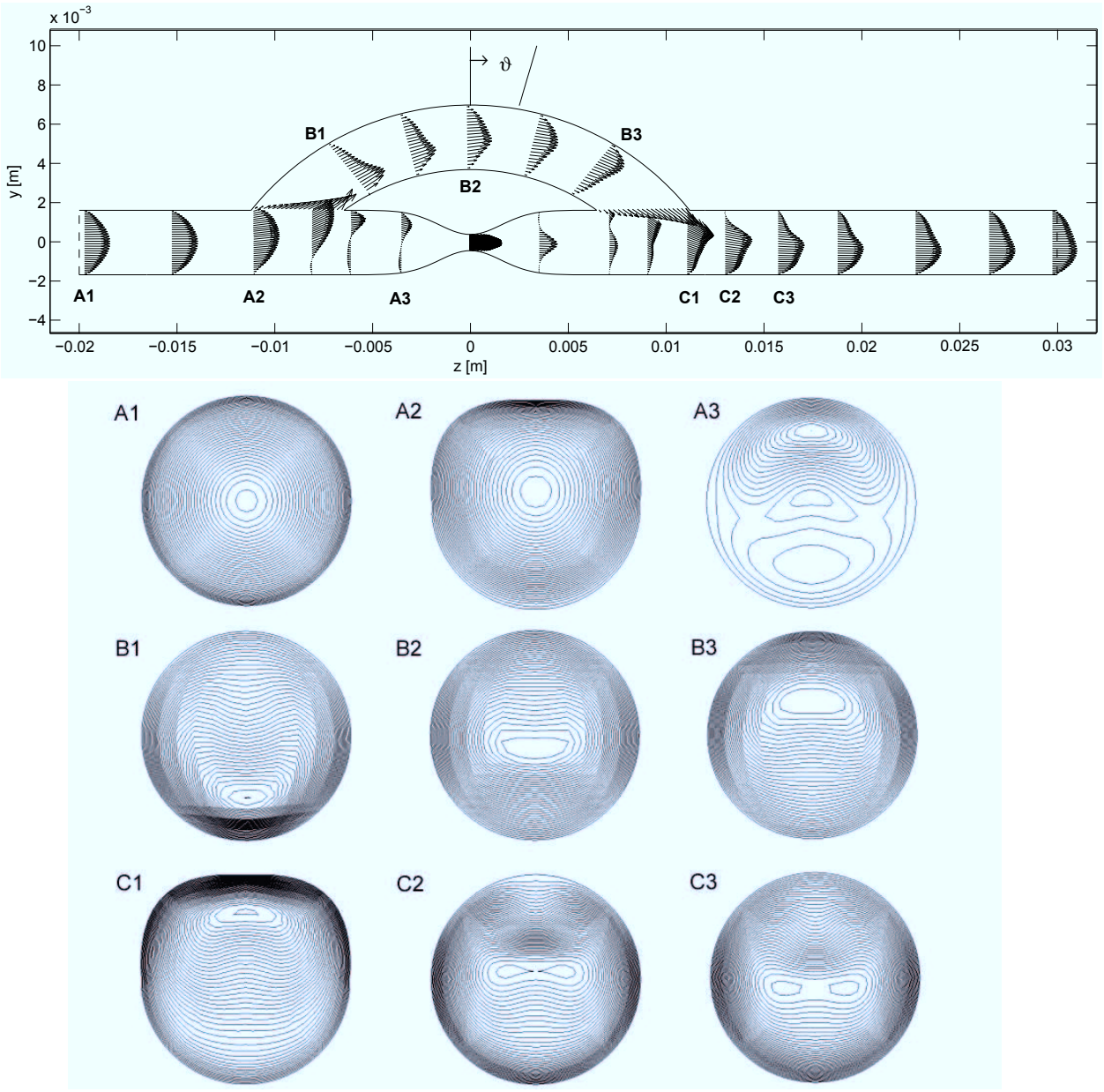

Fig. 7. Velocity profiles in the longitudinal section and iso-velocity contours at selected cross-sections in the stenosed 3D bypass.

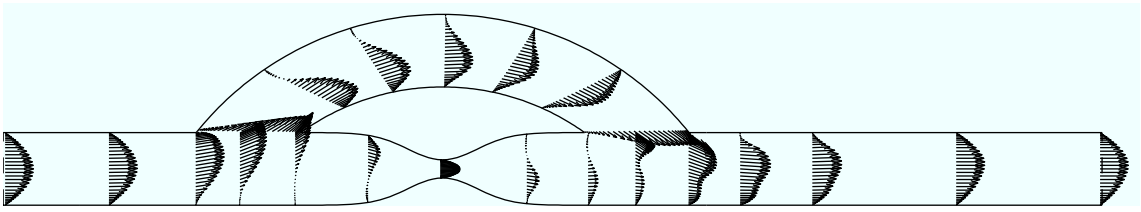

Fig. 8. Velocity profiles at selected cross-sections in the stenosed 2D bypass.

The second bypass type, which was considered in our computations, is the bypass with stenosed artery. It represents the post-operative state, when the residual flow through the stenosis is still present. The resulting velocity distributions in the three-dimensional model are shown

in fig. 7. Similar to the previous bypass type, the velocity profiles in the two-dimensional model are enclosed, fig. 8. At the first sight, the flow pattern of the main stream along the bypass is almost identical to the previous bypass type. The differences in the artery middle and at the distal anastomosis, are caused by the flow through the 75% stenosis. The region upstream from the artery narrowing is characterized by a strong flow near the upper wall and a large recirculation zone in the vicinity of the lower wall (A3). For a more detailed view, see fig. 9, where the low-velocity zones are represented by dark grey color. Another consequence of the stenosis flow is the weaker flow through the bypass graft, which results in less outstanding velocity distribution compared to the occluded bypass.

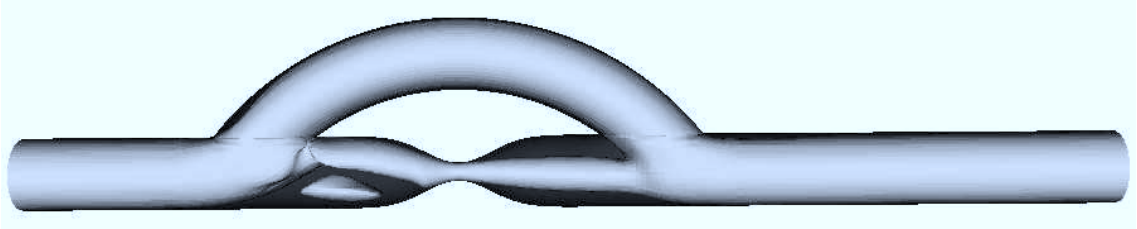

Fig. 9. Distribution of recirculation and low-velocity zones in the stenosed 3D bypass.

The graphs of WSS for the stenosed artery and the bypass graft in the three-dimensional model are shown in fig. 10. By analyzing the graphs, it can be noted that the outstanding peak in the middle of the native artery corresponds to the jet flow through the artery narrowing. Its shape depends on the stenosis degree and on the flow portion, which splits at the bifurcation. Particularly, the region of the proximal anastomosis before the stenosis shows differences in the shear stress distribution at the lower and side walls compared to the occluded bypass. The very low values are mainly caused by the presence of a weak recirculation zone before the artery restriction. In the distal anastomosis, the situation shows similar pattern with the exception of a relatively suppressed recirculation zone next to the toe. On the other hand, the main stream influenced by the residual flow through the stenosis, presents a more fluent process of flow stabilization considering the almost identical shear stress values at the lower and side walls, where the flow gradually adjusts to a fully developed velocity profile.

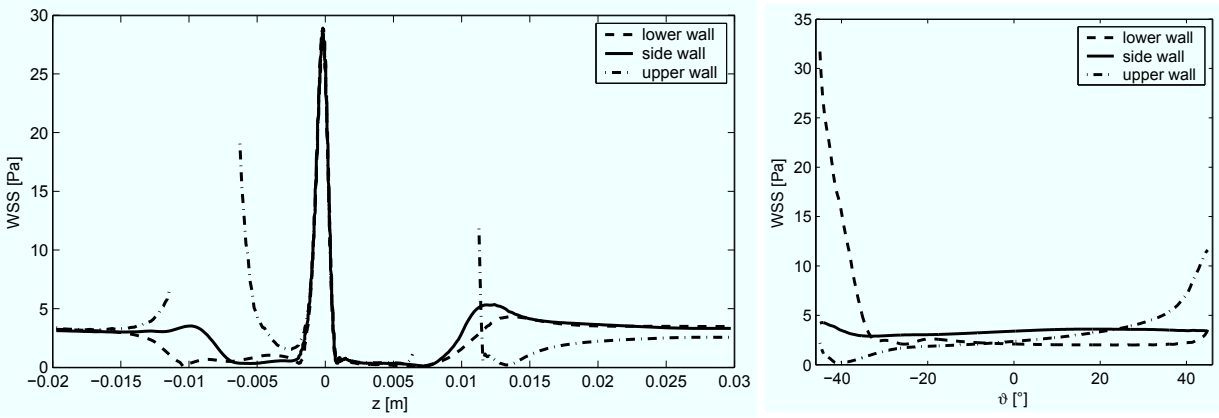

Fig. 10. WSS in the stenosed 3D bypass - native artery (left), bypass graft (right).

5. Conclusion

The analysis of flow fields in an idealized bypass model with either occluded or stenosed native artery, confirmed the importance to differ between both bypass types. Although the distribution of velocity and WSS are mostly similar, the presence of the residual flow through the

75% artery narrowing may strongly influence not only the flow in the distal artery, but also the fluid motion through the bypass graft. The application of the Gaussian function for the stenosis shape, resulted in a more natural flow before and after the stenosis in comparison to the usually considered cosine function. The differences are especially evident by high stenosis degrees. All obtained results are comparable with the ones presented in another studies, e.g. in [8] or [2] for occluded or stenosed bypass, respectively. Considering the significance of the three-dimensional geometry in comparison with the two-dimensional one regardless of the bypass type, the differences in the flow pattern along both models are especially evident in the distribution of recirculation and low-velocity zones, whose size and shape could be mainly noted in the three-dimensional case. Nevertheless, the simplified two-dimensional bypass models represented the first step in understanding of bypass hemodynamics, [10].

The main contribution of this study consists not only in the three-dimensional extension of both occluded and stenosed bypass models and in generation of a relatively suitable grid, but also in the development of a more universal computational software, which enables us to work with unstructured grids. In comparison to similar CFD solvers such as the software package Fluent, the computations demonstrated a better convergence history and all obtained results were less dissipative due to the application of higher-order artificial viscosity of Jameson's type, [6]. One of our future aims regarding the numerical simulations in bypass models, is to develop an unsteady solver that is based on the present algorithm, eventually to include the non-Newtonian behavior of human blood in our computations.

Acknowledgements

This investigation was supported by the research project MSM 4977751303 of the Ministry of Education, Youth and Sports of the Czech Republic.

References

[1] A.S. Anayiotos, P.D. Pedroso, E.C. Eleftheriou, R. Venugopalan, W.K. Holman, Effect of a Flow-Streaming Implant at the Distal Anastomosis of a Coronary Artery Bypass Graft, Annals of Biomedical Engineering 30 (2002) 917-926.

[2] C. Bertolotti, V. Deplano, Three-dimensional numerical simulations of flow through a stenosed coronary bypass, Journal of Biomechanics 33 (2000) 1011-1022.

[3] M. Bonert, J.G. Myers, S. Fremes, J. Williams, C.R. Ethier, A Numerical Study of Blood Flow in Coronary Artery Bypass Graft Side-to-Side Anastomosis, Annals of Biomedical Engineering 30 (2002) 599-611.

[4] A.J. Chorin, A numerical method for solving incompressible viscous flow problems, Journal Computational Physics 2 (1967) 12-26.

[5] C.R. Ethier, D.A. Steinman, X. Zhang, S.R. Karpik, M. Ojha, Flow waveform effects on the end-to-side anastomoic flow patterns, Journal of Biomechanics 31 (1998) 609-617.

[6] A.J. Jameson, W. Schmidt, E. Turkel, Numerical Solution of the Euler Equations by Finite Volume Method Using Runge-Kutta Time-Stepping Schemes, AIAA Paper (1981) 81-1259.

[7] J.P. Ku, C.J. Elkins, C.A. Taylor, Comparison of CFD and MRI Flow and Velocities in an In Vitro Large Artery Bypass Graft Model, Annals of Biomedical Engineering 33 (3) (2005) 257-269.

[8] D. Lee, J.M. Su, H.Y. Liang, A numericla simulation of steady flow fields in a bypass tube, Journal of Biomechanics 34 (2001) 1407-1416.

[9] J. Vimmr, Numerical solution of urine flow in the male urethra, CD-ROM Proceedings of the 10th International Conference on Numerical Methods in Continuum Mechanics, Žilina, 2005.

[10] J. Vimmr, A. Jonášová, Finite volume simulation of blood flow through complete bypass models, Proc. Appl. Math. Mech., 2007. (to appear)